Nanobodies Targeting Mouse/Human VCAM1 for the Nuclear Imaging of Atherosclerotic Lesions

First author's surname and short title:
Broisat - Imaging Atherosclerosis with Anti-VCAM1 Nanobodies

Alexis Broisat[1,], PhD; Sophie Hernot[2,*], PhD; Jakub Toczek[1], MSc; Jens De Vos[2,3,4], MSc; Laurent M. Riou[1], PhD; Sandrine Martin[1], PhD; Mitra Ahmadi[1], PhD; Nicole Thielens[5], Ulrich Wernery[6], PhD; Vicky Caveliers[2,7], PhD; Serge Muyldermans[3,4], PhD, Tony Lahoutte[2,7], MD PhD; Daniel Fagret[1], MD PhD; Catherine Ghezzi[1,*], PhD; Nick Devoogdt[2,*], PhD.*

[1] Radiopharmaceutiques Biocliniques, INSERM, 1039, Université de Grenoble, La Tronche, France
[2] In vivo Cellular and Molecular Imaging Laboratory, Vrije Universiteit Brussel (VUB), Brussels, Belgium
[3] Department of Structural Biology, Vlaams Instituut voor Biotechnologie (VIB), Brussels, Belgium
[4] Laboratory of Cellular and Molecular Immunology, Vrije Universiteit Brussel (VUB), Brussels, Belgium
[5] Laboratoire d'Enzymologie Moléculaire CNRS UMR 5075, IBS, Grenoble, France,
[6] Central Veterinary Research Laboratory, Dubai, United Arab Emirates
[7] Nuclear Medicine Department, UZ Brussel, Brussels, Belgium
[*] Authors contributed equally

Corresponding author:
Alexis Broisat, PhD
Laboratoire des Radiopharmaceutiques Bioclinique
INSERM 1039
Faculté de Médecine de Grenoble
Domaine de la Merci
38700 La Tronche
Fax # +33 4 76 63 71 42
Telephone # +33 4 76 63 71 02
Email address: alexis.broisat@inserm.fr

Total Word Count: 6965
Journal subject codes:
[32] Nuclear cardiology and PET
[124] Cardiovascular imaging agents/Techniques
[144] Other arteriosclerosis
[150] Imaging

Abstract

Rationale. There is a well-recognized need for a noninvasive tool allowing the detection of vulnerable atherosclerotic plaques. By combining nanomolar affinities and fast blood clearance, nanobodies represent potential generic radiotracers for cardiovascular molecular imaging. As an inflammatory marker, Vascular Cell Adhesion Molecule-1 (VCAM1) constitutes a relevant target for molecular imaging of atherosclerotic lesions.
Objective. We aimed to generate, radiolabel and evaluate anti-VCAM1 nanobodies for noninvasive detection of atherosclerotic lesions.
Methods and Results. Ten anti-mouse or anti-mouse/human VCAM1 crossreactive nanobodies with nanomolar affinities were generated, radiolabeled with technetium-99m and screened *in vitro* on mouse and human recombinant VCAM1 proteins and endothelial cells and *in vivo* in ApoE-deficient ($ApoE^{-/-}$) mice. A nontargeting control nanobody was used in all experiments to demonstrate specificity. The lead compound, identified as nanobody cAbVCAM1-5, was found crossreactive for human VCAM1 and exhibited high lesion-to-control (4.95±0.85), lesion-to-heart (8.30±1.11), and lesion-to-blood ratios (4.32±0.48) ($P<0.05$ vs control C57Bl/6J mice for all 3 ratios). Atherosclerotic lesions located within the aortic arch of $ApoE^{-/-}$ mice were successfully identified by SPECT/CT imaging. ^{99m}Tc-cAbVCAM1-5 binding specificity was demonstrated by *in vivo* competition experiments. Autoradiography and immunohistochemistry further confirmed cAbVCAM1-5 uptake in VCAM1-positive lesions.
Conclusions. The ^{99m}Tc-labeled, anti-VCAM1 nanobody cAbVCAM1-5 allowed noninvasive detection of VCAM1 expression and displayed mouse and human crossreactivity. Therefore, this study demonstrates the potential of nanobodies as a new class of radiotracers for cardiovascular applications. The nanobody technology might evolve into an important research tool for targeted imaging of atherosclerotic lesions and has the potential for fast clinical translation.

Keywords: atherosclerosis, imaging, nanobody, nuclear medicine.

Non-standard Abbreviations and Acronyms:
$ApoE^{-/-}$: ApoE-deficient
mVCAM1/hVCAM1: mouse/human vascular cell adhesion molecule-1
ICAM1: intercellular adhesion molecule-1
VLA4: very late antigen-4
kDa: kilodaltons
EGFR: epidermal growth factor receptor
CEA: carcinembryonic antigen
HER2: human epidermal growth factor receptor 2
^{99m}Tc: technetium-99m
V_H: variable domain from conventional antibodies
V_{HH}: variable domain from heavy-chain-only antibodies
RT: reverse transcription
PCR: polymerase chain reaction
RNA: ribonucleic acid
ELISA: enzyme-linked immunosorbent assay
TNFα: tumor necrosis factor alpha
PE: phycoerythrin
mAb: monoclonal antibody
IgG: Immunoglobulin class G
T_m: unfolding temperature
SPR: surface plasmon resonance
HUVEC: human umbillical vein endothelial cells
PBS: phosphate-buffered saline
HPLC: High-performance liquid chromatography
p.i.: post-injection
RP: reverse-phase

ACN: Acetonitrile
TFA: Trifluoroacetic acid
HSA: Human Serum Albumine
i.v.: intravenous
SPECT: Single Photon Emission Computed Tomography
PET: positron emission tomography
CT: (X-ray) Computed Tomography
%ID/g: percent of injected dose per gram
%ID/cm^3: percent of injected dose per cubic centimeter
%ID/TBV: percent of injected dose in total blood volume
DAB: 3,3'-Diaminobenzidine
ROI: region of interest
s.e.m.: standard error of the mean
K_D: equilibrium dissociation constant
nM: nanomolar
Bl: bladder
Kd: kidneys
LN: lymph nodes
Tm: thymus
Sp: spleen
ao: aortic arch
SM: skeletal muscle
SG: salivary glands
BM: bone marrow
ARG: autoradiogram
MIP: maximum intensity projections

Introduction

Several radiotracers of various chemical natures have been evaluated so far for nuclear imaging of atherosclerotic lesions, including lipoproteins, peptides, oligopeptides, antibodies, carbohydrates, antisense nucleotides and nanoparticles[1]. However, none of these radiotracers is currently used in routine clinical practice, mostly because of their inability to reach sufficient lesion-to-background ratios *in vivo*. Indeed, nuclear imaging of vulnerable plaques at the level of coronary arteries remains challenging, mostly because of the small volume of the lesions and their vicinity with the blood containing unbound circulating tracer. Thus, an ideal tracer should combine high affinity and specificity, good solubility and stability and efficient radiolabeling with small size and fast blood clearance, so that high contrast images can be obtained shortly after administration. Nanobodies constitute a promising new class of radiotracers that might adhere to these conditions. Nanobodies are derived from unique heavy-chain-only antibodies that are by nature present in *camelids* and represent the smallest possible (10-15 kDa) functional immunoglobulin-like antigen-binding fragment. Nanobody-based tracers targeting cancer antigens EGFR, CEA or HER2 with (sub)nanomolar affinities have already proven their ability to generate highly-specific contrast images in mouse tumor models[2-5].

The inflammatory process leading to the development of vulnerable atherosclerotic lesions is characterized by extensive recruitment of monocytes and lymphocytes into the arterial wall[6]. Several endothelial adhesion molecules are implicated in the process of leukocyte rolling, firm adhesion and transmigration, such as E- and P-selectins, vascular cell adhesion molecule-1 (VCAM1) and intercellular adhesion molecule-1 (ICAM1)[7]. VCAM1 is a receptor of the immunoglobulin family that binds to very late antigen-4 (VLA4) present on the surface of leukocytes[8]. As active inflammation characterized by leukocyte infiltration is recognized as a major criterion for defining a vulnerable plaque[9], the adhesion molecule VCAM1 is a relevant molecular target for noninvasive detection of such lesions. Indeed, VCAM1 expression was observed at the level of the luminal endothelium as well as on neovessels of advanced lesions, on macrophages and on activated smooth muscle cells[10-12] Therefore, molecular probes targeting VCAM1 have been evaluated by our group and others either for nuclear, magnetic resonance, fluorescent or ultrasound *in vivo* imaging[13-16.]

In the present study, our objectives were to generate and evaluate nanobody-based radiolabeled tracers for preclinical imaging of atherosclerotic plaques. Specifically, we describe 1) the generation and full *in vitro* characterization of crossreactive mouse and human VCAM1-targeted nanobodies; 2) their ^{99m}Tc-radiolabeling; and 3) their thorough assessment as tracers for noninvasive *in vivo* nuclear molecular imaging of atherosclerotic lesions in ApoE-deficient ($ApoE^{-/-}$) mice.

Material and Methods

An exhaustive version of this section is available in the Supplemental data file.

Nanobody generation and production

VCAM1-targeting nanobodies were generated largely following published methods[17]. Specifically, a dromedary was immunized with both mouse and human recombinant VCAM1 proteins (RnD Systems), blood lymphocytes were isolated and RNA purified. The variable domains of the heavy-chain-only antibodies (V_{HH}s or nanobodies) were amplified using a two-step RT-PCR method and cloned in frame with M13 bacteriophage gene 3. Nanobodies were phage-displayed and used in biopannings on immobilized immunogens. Crude bacterial extracts containing soluble nanobodies were used to select individual VCAM1 binders based on a positive signal in ELISA and in flow cytometry on TNFα-stimulated bEND5 cells. After sequencing, selected anti-VCAM1 and irrelevant control cAbBcII10 nanobodies were produced as hexahistidine-tagged proteins in *E. coli* and purified, as described previously[18].

In vitro evaluation of unlabeled nanobodies

Cell lines - The mouse endothelial cell line bEND5 (ECACC) was cultured in supplemented DMEM medium, and the human umbilical vein endothelial cells HUVEC in supplemented EndoGro basal medium (Millipore). VCAM1 expression was induced by stimulation with 10 ng/mL TNFα during

18h.
Flow cytometry –10^5 TNFα-stimulated and unstimulated cells were incubated either with PE-labeled anti-VCAM1 monoclonal antibody (mAb) (anti-mouse from Abcam; anti-human from RnD Systems), or sequentially with 1µg nanobody, 1µg anti-His-tag mAb (Serotec) and 200ng PE-labeled rat anti-mouse IgG1 (BD Biosciences). Binding was measured on a FACS Canto II analyzer (BD Biosciences) and data analyzed with FlowJo software (TreeStar).
Thermal stability – T_m values (unfolding temperatures) were obtained on a J-715 spectropolarimeter (Jasco, Easton, MD, USA), as previously described[4].
Surface Plasmon Resonance (SPR)-based affinity evaluation – Nanobodies affinity for recombinant human and mouse VCAM1 was determined by SPR analysis on a Biacore 3000 apparatus. Recombinant mouse ICAM1 (RnD Systems) was used as a negative control. Recombinant proteins were immobilized on a CM5 sensor chip (Biacore) according to the manufacturer's instructions. A 2-fold dilution series of nanobodies from 50 to 1 nmol/L were tested. Affinity constants were determined using a 1:1 standard association model fit (BIAevaluation software).
Epitope competition using SPR - SPR was used to determine which nanobodies compete for the same epitope. These procedures have been described in detail elsewhere[5].

Radiolabeling and HPLC assessment of *in vitro* and *in vivo* stability
Nanobodies were radiolabeled with ^{99m}Tc using the tricarbonyl-method, as described elsewhere[3]. Radiochemical purity was assessed immediately after labeling, after 6h at 20°C in PBS and in mouse blood 3h post-injection (p.i.). In the latter case, 100µL sampled whole blood was centrifuged and plasma was filtered using a Nanosep 10 kDa Omega Membrane. Radiochemical purity was determined by RP-HPLC using a C4 column eluted with an ACN/TFA gradient mobile phase. Radioactivity was monitored using a radiodetector (γ-RAM Model 4, LabLogic).

***In vitro* evaluation of ^{99m}Tc-labeled nanobodies**
$250x10^3$ bEND5 cells were plated in 24-well plates and stimulated 18h with 10ng/ml TNFα. Five nmol/L of each ^{99m}Tc-nanobody was incubated in 0.5mL PBS + 1% HSA for 1.5h at 37ºC. Competition studies with a 500-fold excess of unlabeled nanobody were conducted to assess the specificity of the binding. After washing, bound ^{99m}Tc-nanobody was collected and counted in a gamma-counter (Canberra Packard). Nonspecific binding to the well was subtracted, and results were normalized to the TNFα-negative condition.

Animal model and processing of aortas
All animal experiments were approved by the Grenoble Research Center of the Army Health Services (CRSSA) committee. 35±2 (mean±SD) week-old female ApoE$^{-/-}$ and control C57Bl/6J mice were used (Charles-River). ApoE$^{-/-}$ mice (n=47) were fed a western diet containing 0.25% cholesterol (Safe) for 18 weeks, whereas control mice (n=15) remained on a standard chow diet.

Biodistribution – Each anti-VCAM1 nanobody was evaluated in 3 ApoE$^{-/-}$ mice except ^{99m}Tc-cAbVCAM1-5 (n=6), which was also further evaluated in control C57Bl/6J mice (n=4). ^{99m}Tc-cAbBcII10 was evaluated as a negative control in both ApoE$^{-/-}$ (n=4) and control mice (n=5). Two hours following ^{99m}Tc-radiolabeled nanobody administration (67±4 MBq i.v.), SPECT/CT acquisition was performed (nanoSPECT, Bioscan, see below). Mice were then euthanized and aortas were cut into 12 segments. A lesion-extension index was attributed to each segment as shown in supplemental Fig. 1: (-) no lesion (control segments), (+) lesion covering up to 50% of the arterial segment length, (++) lesions covering >50% of the arterial segment length and (+++) lesions extending over the whole segment length. Biodistribution results were expressed as a percent of injected dose per gram of tissue (%ID/g). Aortic lesion and control uptakes were defined as the average uptake in all segments ranked (+++) or (-), respectively. Lesion-to-control, lesion-to-blood and lesion-to-heart ratios were also determined. Adjacent 20µm and 8µm-thick cryosections were obtained from all twelve aortic segments for micro-autoradiography imaging (BASS-5000, Fujifilm) and immunohistological VCAM1 staining, respectively.

Competition – Biodistribution of ^{99m}Tc-cAbVCAM1-5 in ApoE$^{-/-}$ mice was assessed by SPECT/CT imaging and *ex vivo* by gamma-well counting with (n=6) or without (n=4) co-injecting a 100-fold excess of unlabeled competitor nanobody cAbVCAM1-1. Results were expressed in %ID/g.
Pharmacodynamics – A subgroup of C57Bl/6J mice was used to evaluate ^{99m}Tc-cAbVCAM1-5 pharmacodynamics in major organs using dynamic SPECT/CT imaging from 0 to 180 min following injection (86.1 ± 28.0 MBq) (n=3). Results were expressed as %ID/cm^3.
Blood kinetics – ^{99m}Tc-cAbVCAM1-5 blood clearance was assessed in C57Bl/6 mice (n=3) by collecting blood samples at several time points after injection. Results were expressed as %ID in total blood volume (%ID/TBV).

Immunohistochemistry
Primary anti-VCAM1 antibody (Santa-Cruz Biotechnology) was applied overnight at 4°C, biotinylated secondary antibody (Jackson ImmunoResearch) was incubated for 1h at 20°C and DAB was used as the chromogen. Staining specificity was assessed by omitting the primary antibody. In a subset of ApoE$^{-/-}$ and control mice, VCAM1 immunostaining was also performed on heart, muscle, salivary gland, liver, bone marrow, lymph node, spleen and thymus.

SPECT/CT imaging
Two hours following i.v. injection, anesthetized animals were placed in a temperature-controlled bed and whole-body SPECT/CT acquisitions were performed from 2 to 3 hours p.i. (nanoSPECT, Bioscan). CT and SPECT acquisitions were reconstructed, fused and quantified using dedicated software (InVivoScope). SPECT scale was normalized to %ID/cm^3 to allow direct visual comparison between animals. Regions of Interest (ROIs) were drawn at the level of the aortic arch and left ventricle cavity for determination of arch-to-blood ratio.

Autoradiography
For each animal, autoradiographic images were obtained following overnight exposure of 3 sets of 20µm thick slices obtained at distinct levels of the 12 aortic segments. Images were quantified using dedicated software (Image Gauge, Fujifilm). ROIs were drawn around atherosclerotic lesions and control VCAM1-negative aortic wall. Results were corrected from background and expressed as average lesion-to-control ratios.

Statistical analysis
All results are presented as mean±s.e.m. Nonparametric Mann & Witney U, Wilcoxon, and Spearman tests were employed to compare unpaired datasets, paired datasets, and correlations between aortic uptake and lesion extension, respectively. Differences were considered significant for $P<0.05$.

Results

Generation of anti-VCAM1 nanobodies

In order to make future clinical translation possible, we aimed at developing nanobodies crossreactive for mouse and human VCAM1. Nanobodies were therefore generated by immunizing a dromedary with both mouse and human VCAM1 recombinant proteins followed by biopannings of the resulting phage-displayed immune nanobody library. Crude bacterial extracts containing individual nanobodies were screened by ELISA for binding to VCAM1 recombinant proteins and in flow cytometry to bind to VCAM1-expressing bEND5 cells (data not shown).

Upon sequencing, 31 different anti-VCAM1 nanobodies were identified that could be grouped into 12 families based on similar sequences in antigen-binding loops. Six nanobody families were mouse VCAM1 (mVCAM1)-specific and 6 families bound to both mouse and human VCAM1 (hVCAM1). Based on ELISA and flow cytometry signals of crude extracts, 10 nanobodies (called cAbVCAM1-1 to -10) were selected for further studies. Nanobody production yield ranged from 0.8 to 10.5mg/L bacterial culture (Table 1). cAbBcII10, binding to a bacterial enzyme[18], was used as a nontargeting control nanobody in further, comparative experiments.

In vitro characterizations

Flow cytometry analysis of mouse bEND5 and human HUVEC endothelial cells stained with an anti-VCAM1 antibody showed low basal VCAM1 expression that was strongly elevated upon TNFα-treatment (Figure 1A-B). Under these conditions, all 10 selected nanobodies interacted with mVCAM1 on stimulated bEND5 cells (Figure 1A). Among them, 6 were found to be crossreactive for hVCAM1 expressed on stimulated HUVECs (Figure 1B). As demonstrated by SPR analyses summarized in Table 1 and as exemplified in Figure 1C, all selected nanobodies bound to mVCAM1 with high affinities ranging from 0.2 to 45.7 nmol/L. Moreover, in accordance with that observed by flow cytometry, 6 nanobodies were found crossreactive for hVCAM1 with affinities remaining in the nanomolar range (Table 1). No binding to the related adhesion receptor ICAM1 was observed for any anti-VCAM1 nanobody, and the control nanobody cAbBcII10 did not bind to VCAM1 in SPR studies. Based on SPR competition studies (supplemental Figure 2), cAbVCAM1 nanobodies could be grouped into 3 epitope-targeting categories: cAbVCAM1-1/5, cAbVCAM1-2/3/6/7/9/10 and cAbVCAM1-4/8. All nanobodies exhibited high thermal stability as demonstrated by unfolding temperatures ranging from 59.4 to >87°C (Table 1).

Following ^{99m}Tc-radiolabeling and purification steps, radiochemical purities were >95% for all nanobodies. ^{99m}Tc-labeling did not affect VCAM1 recognition for most binders as demonstrated by the *in vitro* binding assay on bEND5 cells (Figure 1D): besides cAbVCAM1-8, binding on VCAM1-positive, TNFα-stimulated cells was significantly higher than on unstimulated cells. Moreover, binding on TNFα-stimulated cells was successfully inhibited by competition with an excess of unlabeled nanobody and binding of the negative control cAbBcII10 to either stimulated or untreated cells was negligible, thereby demonstrating specificity.

Immunohistochemistry and biodistribution analyses

As depicted in Figure 2, VCAM1 constitutive expression was observed in lymphoid tissues (i.e. bone marrow, lymph node, spleen and thymus) in both C57Bl/6J control and hypercholesterolemic ApoE$^{-/-}$ mice, whereas no VCAM1 expression was found in heart, muscle and salivary gland. VCAM1 staining was also found in ApoE$^{-/-}$ mice liver. Moreover, strong VCAM1 staining was also observed within aortic lesions at the level of the luminal endothelium, as well as inside the atherosclerotic plaque, but not in the aorta of control C57Bl/6J mice.

Biodistributions of ^{99m}Tc-labeled nanobodies in ApoE$^{-/-}$ mice are summarized in supplemental Table 1. All nanobodies, including control cAbBcII10, exhibited high kidney uptake ranging from 97±16 to 315±33 %ID/g and high activities in the bladder. As expected, ^{99m}Tc-cAbVCAM1 uptakes in VCAM1-positive tissues were higher than that of the nontargeting control ^{99m}Tc-cAbBcII10, a difference which reached statistical significance for ^{99m}Tc-cAbVCAM1-3 (spleen and thymus), ^{99m}Tc-cAbVCAM1-4/5 (spleen, thymus, liver and bone marrow) and ^{99m}Tc-cAbVCAM1-9 (thymus and liver), and ^{99m}Tc-cAbVCAM1-1/8/10 (liver) ($P<0.05$ vs ^{99m}Tc-cAbBcII10). With the exception of the

lung (mean uptake of 2.5±0.8 %ID/g), uptake was lower than 2 %ID/g in other investigated tissues, including the blood and myocardium.

Aortas from hypercholesterolemic ApoE$^{-/-}$ mice injected with ^{99m}Tc-labeled nanobodies were segmented and samples were macroscopically scored according to relative lesion content. As shown in Table 1, uptake in atherosclerotic lesions was greater than 2 %ID/g for 6 out of 10 cAbVCAM1, with a maximum value of 2.99±0.07 %ID/g for ^{99m}Tc-cAbVCAM1-9 ($P<0.05$ vs ^{99m}Tc-cAbBcII10), whereas the lowest uptake was noted for the nontargeting control ^{99m}Tc-cAbBcII10.

Lesion-to-control, lesion-to-blood and lesion-to-heart ratios were determined from biodistribution data (Table 1). Lesion-to-control ratios were >2 for all VCAM1-specific nanobodies with the exception of ^{99m}Tc-cAbVCAM1-8, with a maximum ratio of 4.95±0.85 for ^{99m}Tc-cAbVCAM1-5 ($P<0.05$ vs ^{99m}Tc-cAbBcII10). Lesion-to-blood ratio was >1 for 9 out of 10 ^{99m}Tc-cAbVCAM1 nanobodies, with a maximum ratio of 5.06±0.39 for ^{99m}Tc-cAbVCAM1-3 ($P<0.05$ vs ^{99m}Tc-cAbBcII10). Finally, lesion-to-heart ratio was >1 for all nanobodies, with a maximum value of 8.30±1.11 for ^{99m}Tc-cAbVCAM1-5 ($P<0.05$ vs ^{99m}Tc-cAbBcII10).

Further evaluations of the lead nanobody cAbVCAM1-5

Based on selection criteria summarized in Table 1, cAbVCAM1-5 was selected among the 10 evaluated anti-VCAM1 nanobodies for further investigations and compared to nontargeting control ^{99m}Tc-cAbBcII10.

Stability – As demonstrated by HPLC, ^{99m}Tc-cAbVCAM1-5 was stable *in vitro* for up to 6 h following radiolabeling, as well as *in vivo* in the blood at 3 h post-injection, following completion of SPECT imaging (Figure 3A-C).

Biodistribution.– ^{99m}Tc-cAbVCAM1-5 rapidly cleared from the circulation and background tissues (Supplemental Figure 3) and uptake in kidneys, bladder and VCAM1-positive lymphoid tissues was clearly identifiable on *in vivo* SPECT images from control C57Bl/6J mice, whereas only the kidneys and bladder were visible following the injection of the nontargeting control ^{99m}Tc-cAbBcII10 (Figure 3D and 3E). ^{99m}Tc-cAbVCAM1-5 uptake in lymphoid tissues was further confirmed *ex vivo* by biodistribution analyses (Table 2). Indeed, ^{99m}Tc-cAbVCAM1-5 uptake represented 7.4±0.2, 1.5±0.1 and 7.9±2.0 %ID/g in spleen, thymus and bone marrow of control mice, respectively ($P<0.05$ vs nontargeting control ^{99m}Tc-cAbBcII10). Furthermore, ^{99m}Tc-cAbVCAM1-5 biodistribution in ApoE$^{-/-}$ mice major organs was similar to that observed in C57Bl/6J mice (Table 2, P=NS).

Uptake in atherosclerotic lesions – In ApoE$^{-/-}$ mice, ^{99m}Tc-cAbVCAM1-5 aortic uptake correlated with the lesion-extension index. Indeed, ^{99m}Tc-cAbVCAM1-5 uptake in individual aortic segments increased together with the relative volume of the atherosclerotic lesion, whereas no such gradient was observed for ^{99m}Tc-cAbBcII10 (Sperman rho = 0.894; $P<0.0001$; Figure 4A). ^{99m}Tc-cAbVCAM1-5 uptake in the aorta was further characterized using autoradiography of sections. As shown in Figure 4B and supplemental Fig 4, ^{99m}Tc-cAbVCAM1-5 accumulated within VCAM1-positive atherosclerotic lesions, resulting in a lesion-to-control ratio of 8.7±0.8 ($P<0.05$ vs cAbBcII10).

Following SPECT/CT imaging, ^{99m}Tc-cAbVCAM1-5 uptake was readily visualized on atherosclerotic lesions from the aortic arch of hypercholesterolemic ApoE$^{-/-}$ mice whereas no tracer uptake was observed at the same location in control C57Bl/6J animals or with the nontargeting control ^{99m}Tc-cAbBcII10 in either mouse strain (Figure 5A). As a result, the ^{99m}Tc-cAbVCAM1-5 aortic arch-to-blood ratio from ApoE$^{-/-}$ mice was significantly higher than that observed in C57Bl/6J animals or than that obtained following injection of the nontargeting control nanobody ($P<0.05$) (Figure 5B). Finally, coinjection with an excess of unlabeled cAbVCAM1-1, a nanobody recognizing the same VCAM1-epitope as cAbVCAM1-5 (suppl. Fig 2B), resulted in significant decrease in ^{99m}Tc-cAbVCAM1-5 uptake in liver, lymphoid tissues and atherosclerotic lesions, thereby demonstrating specificity of the signals (Figure 6).

Discussion

This study was designed to generate nanobodies recognizing both mouse and human VCAM1 homologues since such crossreactive binders would be suitable for translation into clinical practice after validation in well-characterized animal models. Ten anti-mVCAM1 nanobodies, including 6 nanobodies crossreactive with hVCAM1, were successfully generated and produced with affinities for mouse and/or human homologue in the nanomolar range. The elevated heat resistance of all tested nanobodies allowed ^{99m}Tc radiolabeling at 50°C with high radiochemical purity (>95%). Furthermore, *in vitro* binding assays on VCAM1-positive mouse endothelial cells revealed that all cAbVCAM1 remained specific mVCAM1-binders after ^{99m}Tc-labeling, with the exception of cAbVCAM1-8. As expected due to their small size, nanobodies exhibited fast blood clearance *in vivo*, resulting in a mean circulating activity of 0.8 %ID/g at 3h p.i. in ApoE$^{-/-}$ mice (range 0.3-1.5 %ID/g). In addition, myocardial background activity was also minimal (mean = 0.4 %ID/g, range 0.3-1.5). These biodistribution kinetics are in accordance with those previously obtained using anti-EGFR and anti-HER2 ^{99m}Tc-labeled nanobodies[3,5]. More importantly, cAbVCAM1 nanobody uptake in aortic atherosclerotic lesions was higher than that of a nontargeting control nanobody cAbBcII10, and this difference reached statistical significance for eight out of the ten evaluated nanobodies. Consequently, with the exception of cAbVCAM1-1, lesion-to-control, lesion-to-blood and lesion-to-heart ratios were all >1, with mean ratios of 3.2, 2.9 and 5.6, respectively.

Uptake in VCAM1-positive tissues. In addition to the expected uptake in atherosclerotic lesions, most cAbVCAM1 nanobodies were taken up by lymphoid tissues in both normal and hypercholesterolemic mice, as demonstrated by biodistribution and *in vivo* SPECT imaging experiments. More specifically, the five cAbVCAM1 nanobodies presenting with the highest affinities for mVCAM1 (cAbVCAM1-2/3/4/5/9, all K_D <2.5 nmol/L), exhibited the highest uptakes in the spleen and bone marrow. Corresponding mVCAM1 constitutive expression was observed by immunohistochemistry in spleen, bone marrow, lymph nodes and thymus. Therefore, cAbVCAM1 binding to lymphoid tissues was likely due to specific VCAM1 binding *in vivo*. VCAM1 constitutive expression in lymphoid tissues has been previously reported by others, either in mouse bone marrow[19], spleen[20], lymph nodes[21]and thymus[22], or in human thymus[23], bone marrow and foetal or activated spleen[24]. Furthermore, specific uptake of radiolabeled anti-VCAM1 antibodies in mouse lymphoid organs has also been demonstrated previously[25, 26]. Finally, an increase in the liver activity of several cAbVCAM1 nanobodies was observed, in accordance with the hepatic expression of VCAM1 that was evidenced in ApoE$^{-/-}$ animals in the present study and elsewhere[27].

Selection of lead compound

Based on the parameters summarized in Table 1, cAbVCAM1-5 was selected as the lead compound among 10 evaluated anti-VCAM1 nanobodies. Indeed, cAbVCAM1-5 exhibited the highest lesion-to-control and lesion-to-heart ratios, as well as a high lesion-to-blood ratio. In addition, cAbVCAM1-5 was crossreactive with hVCAM1 with nanomolar affinities for both mVCAM1 and hVCAM1 as demonstrated by SPR and flow cytometry experiments, a highly relevant result when considering the future potential clinical evaluation of cAbVCAM1-5. Finally, cAbVCAM1-5 also displayed the highest heat resistance and production yield. The absence of lysine residue in the antigen-binding regions was also a criterion for cAbVCAM1-5 selection, since the presence of lysine could be a potential hurdle for future studies requesting coupling chemistry via amino-residues, such as for fluorescent or radiolabeling for PET imaging.

cAbVCAM1-5 *in vivo* imaging

^{99m}Tc-cAbVCAM1-5 was stable *in vitro* for up to 6 h following radiolabeling as well as *in vivo* in mouse blood as demonstrated by HPLC, thereby allowing SPECT/CT imaging at 2-3h post-injection. At this time point, atherosclerotic lesions located within the aortic arch of ApoE$^{-/-}$ mice were successfully identified by SPECT/CT imaging, with low myocardial and blood background activities. *In vivo* blocking experiments demonstrated the specificity of the uptake in VCAM1-expressing tissues. Autoradiography and immunohistochemistry further confirmed that ^{99m}Tc-cAbVCAM1-5 aortic uptake was focalised in VCAM1-positive atherosclerotic lesions. ^{99m}Tc-cAbVCAM1-5 is therefore a

suitable radiotracer for the noninvasive *in vivo* imaging of inflammatory processes occurring in atherosclerotic lesions.

Comparison with other radiotracers.

Other antibody-derived radiotracers have been evaluated recently for the imaging of vulnerable atherosclerotic plaques using SPECT[28, 29]. However, the slow blood clearance of full-sized antibodies resulted in suboptimal target-to-background ratios, therefore emphasizing the need to use antibody fragments (Fab, scFv) or engineered variants. Among the other radiotracers previously evaluated for SPECT or PET imaging of atherosclerotic lesions, ^{18}FDG exhibited an elevated uptake in macrophages, thereby allowing *in vivo* imaging of carotid lesions in humans[30]. However, due to high myocardial background, imaging of coronary lesions remains extremely challenging despite the potential use of a specific diet aimed at lowering myocardial uptake[31]. Similarly, in a mouse model of atherosclerosis, Laitinen *et al.* found that ^{18}FDG myocardial uptake was 18.13±10.59 %ID/g in comparison to 0.41±0.16 %ID/g in atherosclerotic lesions at 1h post-injection[32]. ^{18}F-4V, a VCAM1-targeting peptide-based tracer, has recently been evaluated for PET imaging of vulnerable lesions in mice[15]. Interestingly and similarly to that observed in the present study, ^{18}F-4V uptake was elevated in VCAM1-expressing tissues such as the lymph nodes and spleen, and to a lower extent in the thymus (3.7±0.3, 2.1±0.6 and 0.9±0.3 %ID/g at 4h p.i., respectively); however the potential specificity of this binding was not further discussed by the authors. Advantages of the ^{99m}Tc-labeled nanobody cAbVCAM1-5 over ^{18}F-4V include a more than 40-fold higher affinity for mVCAM1 since the IC_{50} of ^{18}F-4V was 86.6 nmol/L whereas cAbVCAM1-5 Kd was 2.0±0.0 nmol/L. Of note, ^{18}F-4V affinity for hVCAM-1 has not been reported yet. ^{99m}Tc-cAbVCAM1-5 also exhibited a lower uptake at 3h p.i. than ^{18}F-4V at 4h p.i. in background tissues such as the blood (0.5±0.1 vs 1.5±0.4 %ID/g), myocardium (0.2±0.0 vs 0.6±0.2 %ID/g), and control aorta (0.6±0.1 vs 1.3±0.4 %ID/g), resulting in a more favorable lesion-to-control ratio in ApoE$^{-/-}$ mice (4.95±0.85 vs 3.12).

Limitations of nanobody-methodology and clinical translatability

Immunization of a camelid with a target protein of interest probably remains a necessary step since nanobodies from naive or synthetic libraries are mostly of lower affinity. In addition, whereas the obtention of recombinant proteins corresponding to large extracellular domains of type I or II transmembrane receptors can be easily achieved, as is the case for VCAM1, the same does not hold for more complex structures such as heterodimeric receptors or receptors spanning the cellular membrane multiple times.

When produced as recombinant proteins, evident questions arise regarding immunogenicity, toxicity and safety when nanobody-based tracers are designed for clinical translation. In this regards, it should be noted that several nanobodies, including an anti-von Willebrand Factor nanobody for prevention of the acute coronary syndromes, were already clinically evaluated in phase Ia, Ib, and II clinical trials without demonstrating adverse events and detectable immunogenicity at repeatedly administered therapeutic doses far above the single injected dose that will be used for diagnostic purposes as described in the present study[33]. Also, we are currently running a 'first-in man' phase I clinical study with a ^{68}Ga-labeled anti-HER2 nanobody[5] for PET imaging of breast cancer patients, in which efficacy, safety and dosimetry will be the monitored parameters.

Conclusions and perspectives

Unlike anatomical imaging methodologies which are confronted with strong resolution requirements in order to distinguish distinct plaque components for the identification of vulnerable lesions based on the size of the necrotic core or the thickness of the fibrous cap, the challenges associated with atherosclerosis molecular imaging are strongly related to the sensitivity of the detection systems. Nuclear imaging presents an exquisite, femtomolar sensitivity which is well-suited for the molecular imaging of atherosclerotic lesions. This study evaluated for the first time the potential of nanobodies as radiotracers dedicated to nuclear cardiology. When taken into perspective with previously published results related to tumor imaging, our results confirm that nanobodies constitute a promising new class of radiotracers with great potential for noninvasive nuclear imaging.

In the present study, ten anti-VCAM1 nanobodies were evaluated. Procedures were carefully designed in order to generate nanobodies crossreactive for hVCAM1 protein. ^{99m}Tc-cAbVCAM1-5 was selected as the most potent candidate for the development of a new radiopharmaceutical for noninvasive imaging of vulnerable atherosclerotic lesions. In ApoE$^{-/-}$ atherosclerotic mice, VCAM1-positive lesions were successfully identified by SPECT/CT imaging using the human & mouse crossreactive ^{99m}Tc-cAbVCAM1-5, thereby demonstrating a strong potential for clinical translation.

In addition to high production yield, high stability and fast blood clearance, nanobodies engineering offers a number of advantages. Specifically, successful radiolabeling of nanobodies with a positron emitter was recently described[2], as well as labeling of nanobodies with near infrared dyes[34] and coupling to microbubbles[35] or Gadolinium-vesicles[36], hereby allowing the use of SPECT, PET, optical, ultrasound or magnetic resonance imaging systems with nanobody-based tracers. In addition, humanized and bivalent nanobodies can easily be generated[4, 37]. In particular, further studies will be conducted to evaluate the performances of bivalent cAbVCAM1 constructs targeted at two distinct epitopes as well as the potential of ^{68}Ga- or ^{18}F-labeled cAbVCAM1-5 for PET imaging of atherosclerotic lesions.

Acknowledgements
We thank I. Bally from the IBS platform of the Partnership for Structural Biology for access to the Biacore facility.

Funding Sources
Jens De Vos has a Ph.D. fellowship of the Research Foundation - Flanders (FWO). Tony Lahoutte is a Senior Clinical Investigator of the Research Foundation Flanders (Belgium) (FWO). The research at ICMI is funded by the Interuniversity Attraction Poles Program, Belgian State and Belgian Science Policy.

Disclosures
None

References

1. Riou LM, Broisat A, Dimastromatteo J, Pons G, Fagret D, Ghezzi C. Pre-clinical and clinical evaluation of nuclear tracers for the molecular imaging of vulnerable atherosclerosis: an overview. *Curr Med Chem*. 2009;16:1499-511.

2. Vosjan MJ, Perk LR, Roovers RC, Visser GW, Stigter-van Walsum M, van Bergen En Henegouwen PM, van Dongen GA. Facile labelling of an anti-epidermal growth factor receptor Nanobody with (68)Ga via a novel bifunctional desferal chelate for immuno-PET. *Eur J Nucl Med Mol Imaging*. 2011;38:753-63.

3. Gainkam LO, Huang L, Caveliers V, Keyaerts M, Hernot S, Vaneycken I, Vanhove C, Revets H, De Baetselier P, Lahoutte T. Comparison of the biodistribution and tumor targeting of two 99mTc-labeled anti-EGFR nanobodies in mice, using pinhole SPECT/micro-CT. *J Nucl Med*. 2008;49:788-95.

4. Vaneycken I, Govaert J, Vincke C, Caveliers V, Lahoutte T, De Baetselier P, Raes G, Bossuyt A, Muyldermans S, Devoogdt N. In vitro analysis and in vivo tumor targeting of a humanized, grafted nanobody in mice using pinhole SPECT/micro-CT. *J Nucl Med*. 2010;51:1099-106.

5. Vaneycken I, Devoogdt N, Van Gassen, N, Vincke C, Xavier C, Wernery U, Muyldermans S, Lahoutte T, Caveliers V. Pre-clinical screening of anti-HER2 Nanobodies for molecular imaging of breast cancer. *FASEB J*. 2011;25:2433-46.

6. Ross R. Atherosclerosis--an inflammatory disease. *N Engl J Med*. 1999;340:115-26.

7. Huo Y, Ley K. Adhesion molecules and atherogenesis. *Acta Physiol Scand*. 2001;173:35-43.

8. Osborn L, Hession C, Tizard R, Vassallo C, Luhowskyj S, Chi-Rosso G, Lobb R. Direct expression cloning of vascular cell adhesion molecule 1, a cytokine-induced endothelial protein that binds to lymphocytes. *Cell*. 1989;59:1203-11.

9. Fuster V, Moreno PR, Fayad ZA, Corti R, Badimon JJ. Atherothrombosis and high-risk plaque: part I: evolving concepts. *J Am Coll Cardiol*. 2005;46:937-54.

10. Iiyama K, Hajra L, Iiyama M, Li H, DiChiara M, Medoff BD, Cybulsky MI. Patterns of vascular cell adhesion molecule-1 and intercellular adhesion molecule-1 expression in rabbit and mouse atherosclerotic lesions and at sites predisposed to lesion formation.Circ Res. 1999; 9:215-219.

11. O'Brien KD, Allen MD, McDonald TO, Chait A, Harlan JM, Fishbein D, McCarty J, Ferguson M, Hudkins K, Benjamin CD, et al.Vascular cell adhesion molecule-1 is expressed in human coronary atherosclerotic plaques. Implications for the mode of progression of advanced coronary atherosclerosis. J Clin Invest. 1993; 92:945-951.

12. O'Brien KD, McDonald TO, Chait A, Allen MD, Alpers CE. Neovascular expression of E-selectin, intercellular adhesion molecule-1, and vascular cell adhesion molecule-1 in human atherosclerosis and their relation to intimal leukocyte content. Circulation. 1996; 93:672-682.

13. Broisat A, Riou LM, Ardisson V, Boturyn D, Dumy P, Fagret D, Ghezzi C. Molecular imaging of vascular cell adhesion molecule-1 expression in experimental atherosclerotic plaques with radiolabelled B2702-p. *Eur J Nucl Med Mol Imaging*. 2007;34:830-40.

14. Nahrendorf M, Jaffer FA, Kelly KA, Sosnovik DE, Aikawa E, Libby P, Weissleder R. Noninvasive vascular cell adhesion molecule-1 imaging identifies inflammatory activation of cells in atherosclerosis. *Circulation*. 2006;114:1504-11.

15. Nahrendorf M, Keliher E, Panizzi P, Zhang H, Hembrador S, Figueiredo JL, Aikawa E, Kelly K, Libby P, Weissleder R. 18F-4V for PET-CT imaging of VCAM-1 expression in atherosclerosis. *JACC Cardiovasc Imaging*. 2009;2:1213-22.

16. Kaufmann BA, Sanders JM, Davis C, Xie A, Aldred P, Sarembock IJ, Lindner JR. Molecular imaging of inflammation in atherosclerosis with targeted ultrasound detection of vascular cell adhesion molecule-1. *Circulation*. 2007;116:276-84.

17. Arbabi Ghahroudi M, Desmyter A, Wyns L, Hamers R, Muyldermans S. Selection and identification of single domain antibody fragments from camel heavy-chain antibodies. *FEBS Lett*. 1997;414:521-6.

18. Saerens D, Pellis M, Loris R, Pardon E, Dumoulin M, Matagne A, Wyns L, Muyldermans S, Conrath K. Identification of a universal VHH framework to graft non-canonical antigen-binding loops of camel single-domain antibodies. *J Mol Biol*. 2005;352:597-607.

19. Levesque JP, Takamatsu Y, Nilsson SK, Haylock DN, Simmons PJ. Vascular cell adhesion molecule-1 (CD106) is cleaved by neutrophil proteases in the bone marrow following hematopoietic progenitor cell mobilization by granulocyte colony-stimulating factor. *Blood*. 2001;98:1289-97.

20. Borrello MA, Phipps RP. Differential Thy-1 expression by splenic fibroblasts defines functionally distinct subsets. *Cell Immunol*. 1996;173:198-206.

21. Boscacci RT, Pfeiffer F, Gollmer K, Sevilla AI, Martin AM, Soriano SF, Natale D, Henrickson S, von Andrian UH, Fukui Y, Mellado M, Deutsch U, Engelhardt B, Stein JV. Comprehensive analysis of lymph node stroma-expressed Ig superfamily members reveals redundant and nonredundant roles for ICAM-1, ICAM-2, and VCAM-1 in lymphocyte homing. *Blood*. 2010;116:915-25.

22. Lepique AP, Palencia S, Irjala H, Petrie HT. Characterization of vascular adhesion molecules that may facilitate progenitor homing in the post-natal mouse thymus. *Clin Dev Immunol*. 2003;10:27-33.

23. Salomon DR, Crisa L, Mojcik CF, Ishii JK, Klier G, Shevach EM. Vascular cell adhesion molecule-1 is expressed by cortical thymic epithelial cells and mediates thymocyte adhesion. Implications for the function of alpha4beta1 (VLA4) integrin in T-cell development. *Blood*. 1997;89:2461-71.

24. Schweitzer KM, Drager AM, van der Valk P, Thijsen SF, Zevenbergen A, Theijsmeijer AP, van der Schoot CE, Langenhuijsen MM. Constitutive expression of E-selectin and vascular cell adhesion molecule-1 on endothelial cells of hematopoietic tissues. *Am J Pathol*. 1996;148:165-75.

25. Dyer CM, Lew AM. Antigen targeted to secondary lymphoid organs via vascular cell adhesion molecule (VCAM) enhances an immune response. *Vaccine*. 2003;21:2115-21.

26. Jacobsen K, Kravitz J, Kincade PW, Osmond DG. Adhesion receptors on bone marrow stromal cells: in vivo expression of vascular cell adhesion molecule-1 by reticular cells and sinusoidal endothelium in normal and gamma-irradiated mice. *Blood*. 1996;87:73-82.

27. Yin M, Zhang L, Sun XM, Mao LF, Pan J. Lack of apoE causes alteration of cytokines expression in young mice liver. *Mol Biol Rep*. 2010;37:2049-54

28. Temma T, Ogawa Y, Kuge Y, Ishino S, Takai N, Nishigori K, Shiomi M, Ono M, Saji H. Tissue factor detection for selectively discriminating unstable plaques in an atherosclerotic rabbit model. *J Nucl Med*. 2010;51:1979-86.

29. Kuge Y, Takai N, Ogawa Y, Temma T, Zhao Y, Nishigori K, Ishino S, Kamihashi J, Kiyono Y, Shiomi M, Saji H. Imaging with radiolabelled anti-membrane type 1 matrix metalloproteinase (MT1-MMP) antibody: potentials for characterizing atherosclerotic plaques. *Eur J Nucl Med Mol Imaging*. 2010;37:2093-104.

30. Rudd JH, Warburton EA, Fryer TD, Jones HA, Clark JC, Antoun N, Johnstrom P, Davenport AP, Kirkpatrick PJ, Arch BN, Pickard JD, Weissberg PL. Imaging atherosclerotic plaque inflammation with [18F]-fluorodeoxyglucose positron emission tomography. *Circulation*. 2002;105:2708-11.

31. Wykrzykowska J, Lehman S, Williams G, Parker JA, Palmer MR, Varkey S, Kolodny G, Laham R. Imaging of inflamed and vulnerable plaque in coronary arteries with 18F-FDG PET/CT in patients with suppression of myocardial uptake using a low-carbohydrate, high-fat preparation. *J Nucl Med*. 2009;50:563-8.

32. Laitinen I, Marjamaki P, Haaparanta M, Savisto N, Laine VJ, Soini SL, Wilson I, Leppanen P, Yla-Herttuala S, Roivainen A, Knuuti J. Non-specific binding of [18F]FDG to calcifications in atherosclerotic plaques: experimental study of mouse and human arteries. *Eur J Nucl Med Mol Imaging*. 2006;33:1461-7.

33. Van Bockstaele F, Holz JB, Revets H. The development of nanobodies for therapeutic applications. *Curr Opin Investig Drugs*. 2009;10:1212-24.

34. Oliveira S, van Dongen GA, Stigter-van Walsum M, Roovers RC, Stam JC, Mali W, van Diest PJ, van Bergen En Henegouwen PM. Rapid Visualization of Human Tumor Xenografts through Optical Imaging with a Near-infrared Fluorescent Anti-Epidermal Growth Factor Receptor Nanobody. Mol Imaging. 2011 Jun 2. [Epub ahead of print]

35. Hernot S, Unnikrishnan S, Du Z, Shevchenko T, Cosyns B, Broisat A, Toczek J, Caveliers V, Muyldermans S, Lahoutte T, Klibanov AL, Devoogdt N.Nanobody-coupled microbubbles as novel molecular tracer. J Control Release. 2011 Dec 16. [Epub ahead of print].

36. Iqbal U, Albaghdadi H, Nieh MP, Tuor UI, Mester Z, Stanimirovic D, Katsaras J, Abulrob A. Small unilamellar vesicles: a platform technology for molecular imaging of brain tumors. Nanotechnology. 2011 May 13;22(19):195102. Epub 2011 Mar 24.

37. Tijink BM, Laeremans T, Budde M, Stigter-van Walsum M, Dreier T, de Haard HJ, Leemans CR, van Dongen GA. Improved tumor targeting of anti-epidermal growth factor receptor Nanobodies through albumin binding: taking advantage of modular Nanobody technology. *Mol Cancer Ther*. 2008;7:2288-97.

TABLES

Table 1.

Radiotracer	%ID/g lesion	Lesion:control	Lesion :blood	Lesion:Heart	K_D mVCAM1 (nmol/L)	K_D hVCAM1 (nmol/L)	Production yield (mg/L)	T_m (°C)
cAbVCAM1-1	0.87±0.08 #9	2.15±0.20 #9	0.74±0.10* #10	2.65±0.23* #9	8.3±1.2 #7	12.4±0.5 #5	2.0 #7	72.3±0.1 #2
cAbVCAM1-2	2.15±0.29* #6	2.90±0.45 #6	3.37±0.32* #5	5.55±0.58* #7	0.3±0.0 #2	Not cross-reactive	5.0 #5	62.3±0.1 #6
cAbVCAM1-3	2.95±0.16* #2	4.07±0.56 #3	5.06±0.39* #1	7.40±0.91* #3	2.4±0.1 #5	9.1±0.9 #4	6.8 #3	59.7±0.1 #9
cAbVCAM1-4	2.21±0.59* #5	3.20±0.74 #5	1.41±0.29 #9	1.96±0.56* #10	0.2±0.0 #1	Not cross-reactive	6.8 #3	59.4±0.1 #10
cAbVCAM1-5	2.53±0.08* #3	4.95±0.85* #1	4.32±0.48* #2	8.30±1.11* #1	2.0±0.0 #4	6.5±0.7 #3	10.5 #1	>87 #1
cAbVCAM1-6	0.73±0.08 #10	4.57±0.93* #2	1.85±0.37 #8	4.98±0.75 #8	5.2±0.6 #6	Not cross-reactive	3.0 #6	72.0±0.1 #3
cAbVCAM1-7	1.27±0.25* #8	2.88±0.65 #7	4.02±1.05* #3	5.98±0.96 #4	26.6±1.2 #9	Not cross-reactive	6.9 #2	60.9±0.3 #8
cAbVCAM1-8	2.48±0.46* #4	1.40±0.10 #10	3.66±0.10* #4	7.71±0.38* #2	13.2±0.3 #8	1.4±0.5 #1	1.5 #8	61.5±0.1 #7
cAbVCAM1-9	2.99±0.07* #1	2.19±0.60 #8	2.51±0.03* #6	5.69±0.36* #6	0.9±0.2 #3	5.3±0.7 #2	0.9 #9	66.8±0.2 #4
cAbVCAM1-10	1.93±0.14* #7	3.47±0.67* #4	2.01±0.14* #7	5.76±0.56* #5	45.7±20.0 #10	18.4±7.0 #6	0.8 #10	63.4±0.2 #5
cAbBcII10	0.68±0.06	1.66±0.28	1.57±0.09	4.00±0.14	ND	ND	5.0	77.5±0.2

Table 1. Comparison between 10 evaluated anti-VCAM1 nanobodies. Mean ± s.e.m. and rank (#) are given for parameters obtained either *ex vivo* by gamma-well counting (%ID/g lesion, Lesion-to-Control ratio, Lesion-to-Blood ratio, Lesion-to-Heart ratio), or *in vitro* (K_D for mVCAM1 or hVCAM1, Production yield and T_m). cAbVCAM1-5 is the most potent candidate based on these criterions. * $P<0.05$ vs cAbBcII10. ND, not detectable.

Table 2.

	^{99m}Tc-cAbBcII10		^{99m}Tc-cAbVCAM1-5	
	C57Bl6/J	ApoE$^{-/-}$	C57Bl6/J	ApoE$^{-/-}$
Blood	0.4±0.0	0.4±0.0	0.5±0.1	0.6±0.1
Heart	0.1±0.0	0.2±0.0	0.2±0.0*	0.3±0.1*
Lung	0.8±0.2	1.0±0.1	1.7±0.2*	2.3±0.3*
Liver	1.0±0.1	0.6±0.0†	1.4±0.2	1.8±0.3*
SM	0.1±0.0	0.1±0.0	0.1±0.0	0.1±0.0
SG	0.3±0.0	0.2±0.0	0.5±0.0*	0.5±0.1*
Thyroid	0.5±0.1	0.4±0.1	0.7±0.1	0.7±0.1
Stomach	0.4±0.0	0.4±0.1	0.5±0.0*	0.6±0.1*
Bile	0.5±0.1	0.4±0.1	0.3±0.0	0.7±0.2
Kidney	350±16	267±14†	287±43	222±12
Spleen	0.3±0.0	0.4±0.0	7.4±0.2*	9.2±1.0*
Thymus	0.1±0.0	0.2±0.0	1.5±0.1*	1.7±0.1*
BM	0.4±0.0	1.0±0.7	7.9±2.0*	10.7±2.9*

Ex vivo biodistribution of ^{99m}Tc-labeled cAbBcII10 and cAbVCAM1-5 nanobodies 3h post-injection in C57Bl/6J and ApoE$^{-/-}$ mice. Results are expressed as mean ± s.e.m. * $P<0.05$ vs strain-matched cAbBcII10. † $P<0.05$ vs C57Bl6/J. SM, skeletal muscle; SG, salivary glands; BM, bone marrow.

Figures

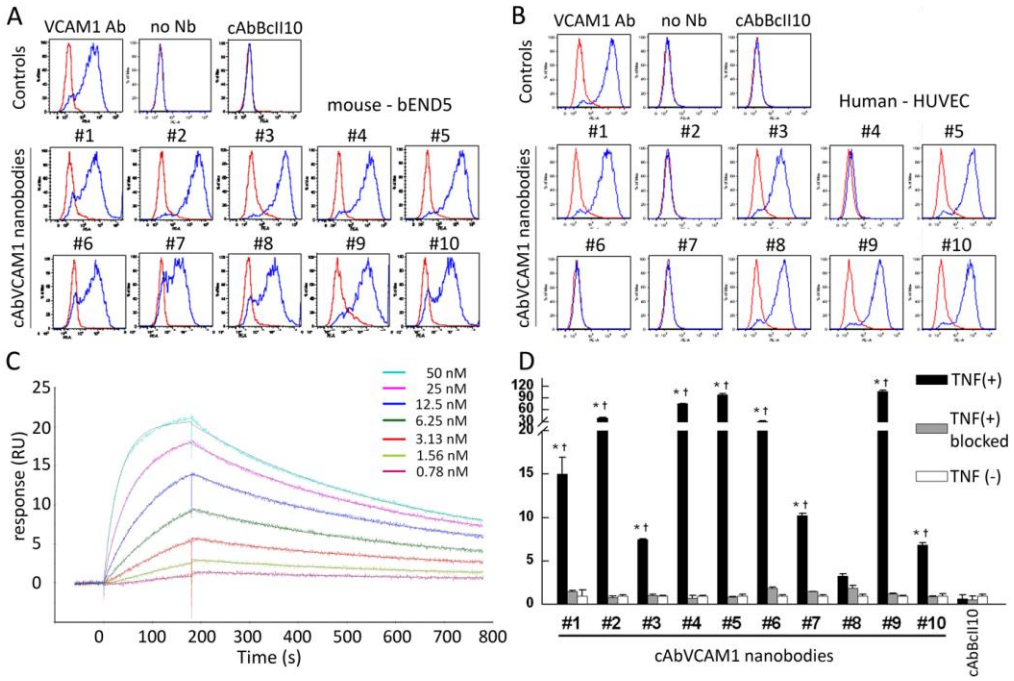

Figure 1. Functionality assessment of anti-VCAM1 nanobodies.
A and B: Flow cytometry analysis of anti-VCAM1 nanobodies on untreated VCAM1-negative (red) and TNFα-treated VCAM1-positive (blue) mouse bEND5 (A) or human HUVEC endothelial cells (B) (x: PE-A, log scale; y: %max). PE-labeled anti-VCAM1 monoclonal antibody was used as a positive control, whereas no nanobody and cAbBcII10 were used as negative controls. All 10 anti-VCAM1 nanobodies bound to mouse VCAM1-positive cells (A), and 6 out of 10 nanobodies were found to be crossreactive for human VCAM1-positive cells (B); C: Representative sensogram of cAbVCAM1-5 binding to mouse VCAM1. D: ^{99m}Tc-nanobodies bound to VCAM1-positive, TNFα-stimulated bEND5 cells. ^{99m}Tc-cAbVCAM1 binding to stimulated cells was significantly higher than binding to unstimulated cells, except for ^{99m}Tc-cAbVCAM1-8. Binding was successfully blocked by an excess of unlabeled nanobody, thereby demonstrating specificity. * P<0.05 vs ^{99m}Tc-cAbBcII10. † P<0.05 vs TNF (+) blocked condition.

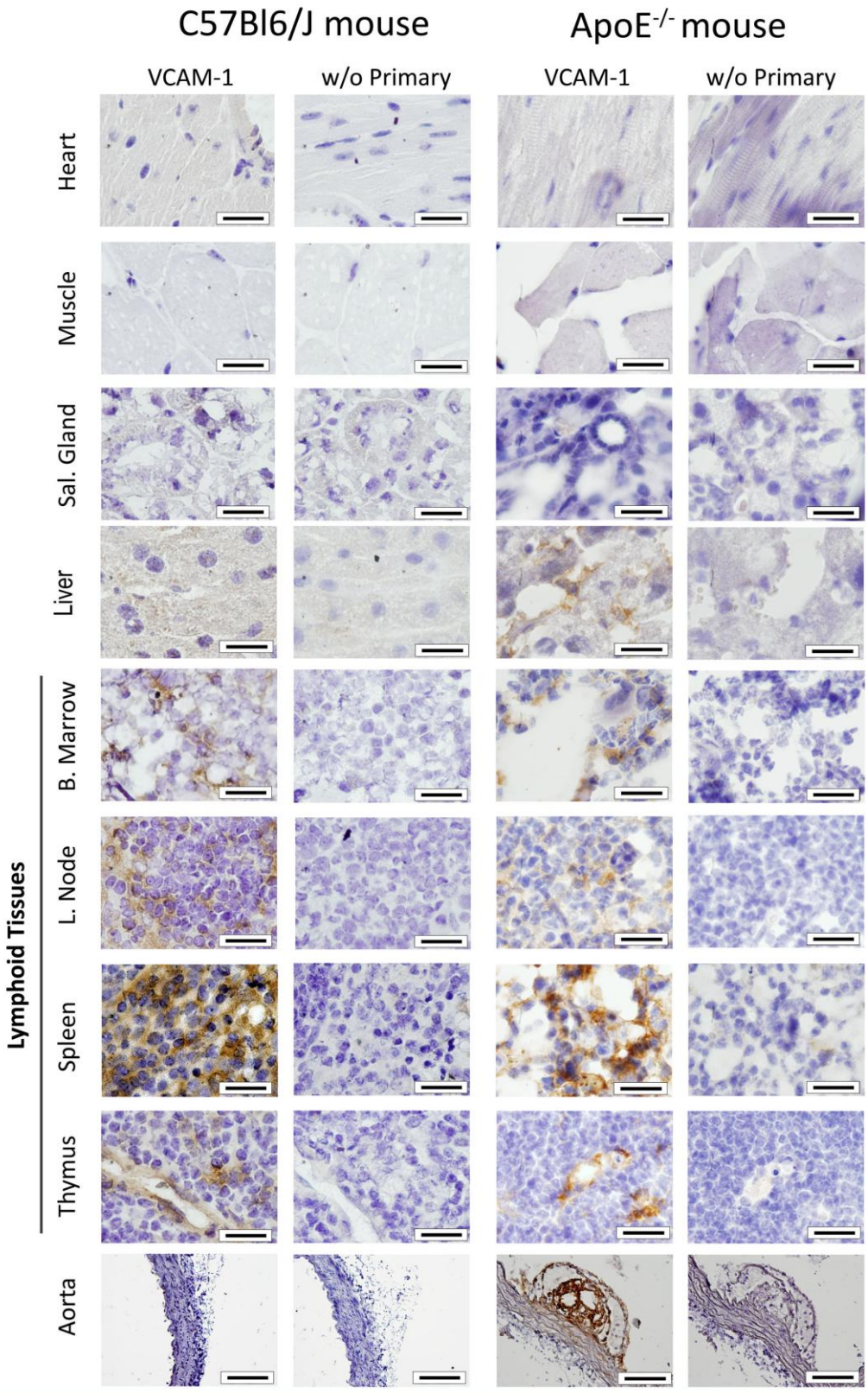

Figure 2. VCAM1 expression was observed in lymphoid tissues (i.e. bone marrow, lymph nodes, spleen and thymus) of both C57Bl/6J control and hypercholesterolemic ApoE$^{-/-}$ mice via immunohistochemistry, whereas no VCAM1 expression was found in heart, muscle and salivary glands. VCAM1 expression was also found in ApoE$^{-/-}$ mice liver. Furthermore, strong VCAM1 expression was observed within aortic lesions, at the level of the endothelium, as well as inside the atherosclerotic plaque. The specificity of these results was demonstrated by the absence of staining on control slices where primary antibody was omitted. Scale bars: 20µm, except for aorta (100µm).

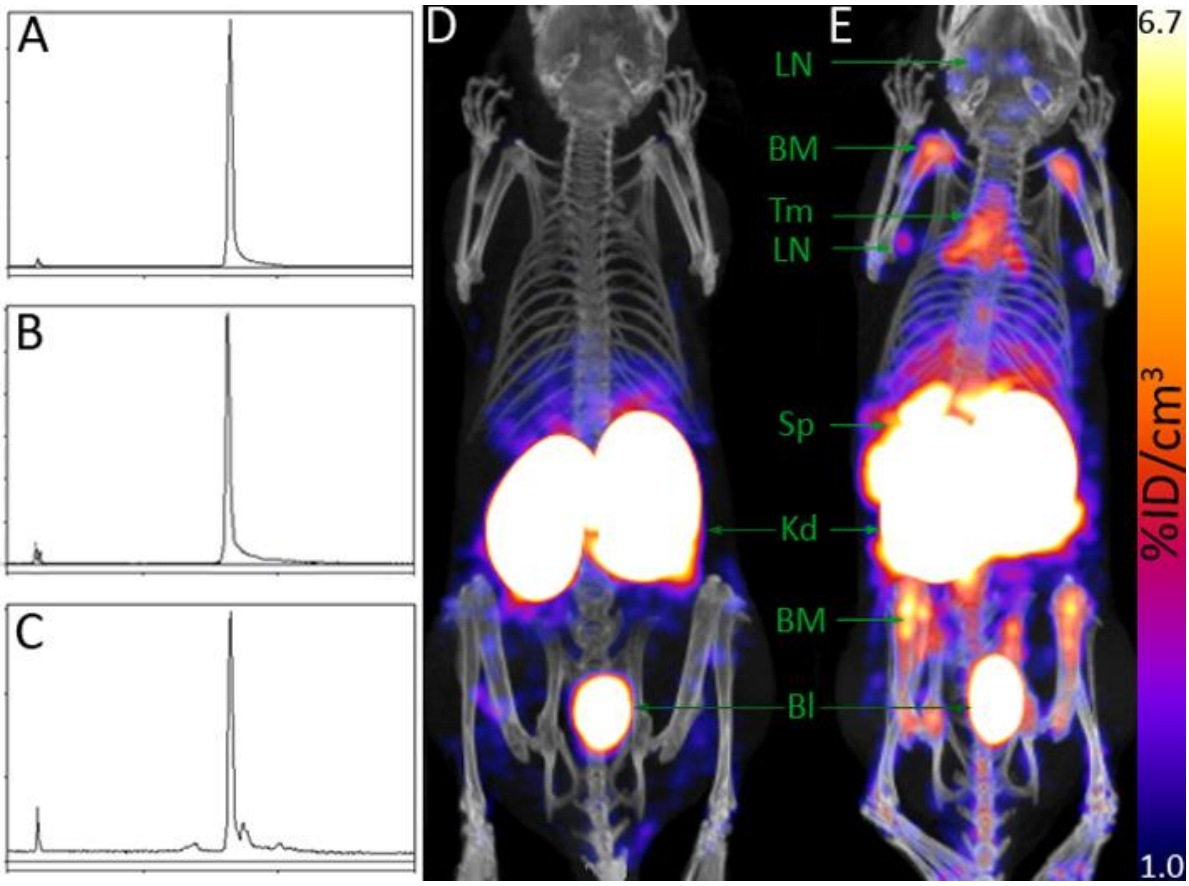

Figure 3.
^{99m}Tc-cAbVCAM1-5 HPLC profiles indicating that this nanobody was stable *in vitro* at 0 (A) and 6 hours (B) following radiolabeling, as well as *in vivo* in the blood 3 hours post-injection (C). Representative *in vivo* SPECT/CT whole body maximum intensity projections images (MIP) of control ^{99m}Tc-cAbBcII10 (D) and ^{99m}Tc-cAbVCAM1-5 (E) nanobodies obtained 2-3h following i.v. injection in C57Bl/6J mice. ^{99m}Tc-cAbVCAM1-5 was taken up at the level of the bladder (Bl) and kidneys (Kd) as well as in the lymphoid tissues : lymph nodes (LN), bone marrow (BM), thymus (Tm) and spleen (Sp).

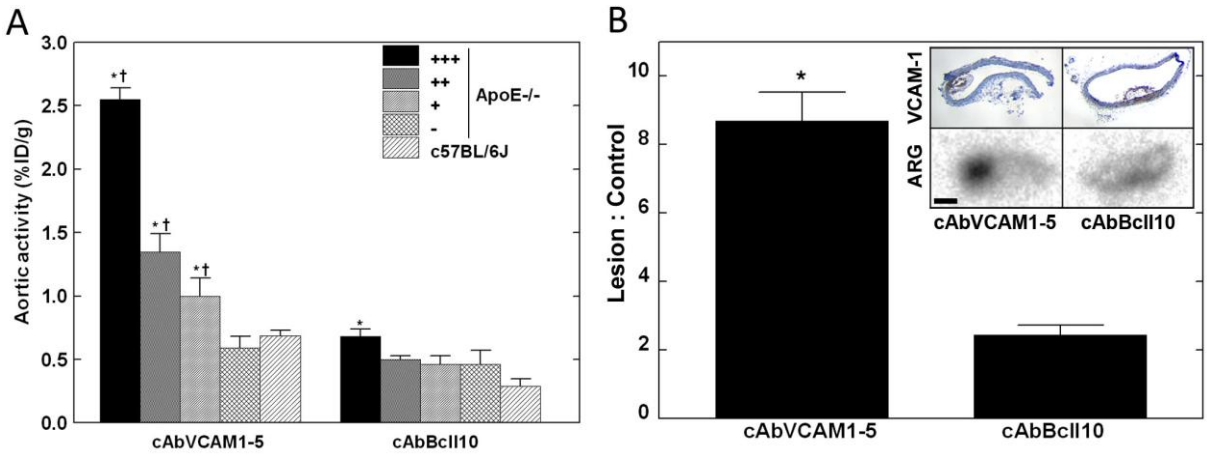

Figure 4.

^{99m}Tc-cAbVCAM1-5 aortic distribution and autoradiography. A: ^{99m}Tc-cAbVCAM1-5 and ^{99m}Tc-cAbBcII10 aortic uptake in arterial segments from ApoE$^{-/-}$ mice ranked according to the lesion-extension index, and in C57Bl/6J control mice aorta. * P<0.05 vs C57Bl/6J, † P<0.05 vs next lesion-extension index. B: Representative ^{99m}Tc-cAbVCAM1-5 and ^{99m}Tc-cAbBcII10 autoradiograms (ARG) are presented together with VCAM1 immunostainings obtained on adjacent slices, showing hot-spot uptake of ^{99m}Tc-cAbVCAM1-5 in VCAM1-positive lesions. Scale bar: 200µm. (* P<0.05 vs. cAbBcII10).

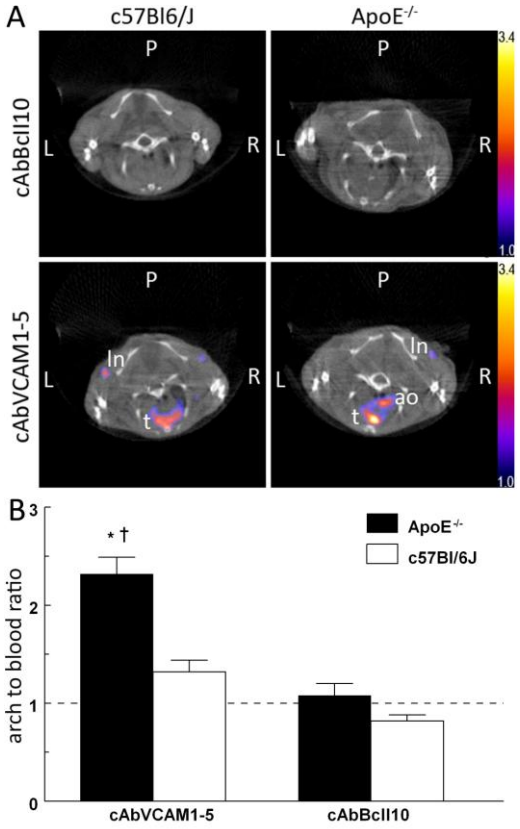

Figure 5.
^{99m}Tc-cAbVCAM1-5 as tracer for SPECT/CT *in vivo* imaging of atherosclerotic plaques. A: Representative *in vivo* SPECT/CT coronal views taken at the level of the aortic arch of C57Bl/6J and ApoE$^{-/-}$ mice 2-3h after i.v. injection of ^{99m}Tc-cAbBcII10 or ^{99m}Tc-cAbVCAM1-5 nanobodies. The scale was adjusted from 1 to 3.4 percent of the injected dose to allow direct visual comparison. Focal uptake of ^{99m}Tc-cAbVCAM1-5 was visible in the axillary lymph nodes (ln) and thymus (t) of both C57Bl/6J and ApoE$^{-/-}$ mice. In addition, ^{99m}Tc-cAbVCAM1-5 uptake in atherosclerotic lesions from ApoE$^{-/-}$ mice was also clearly identifiable at the level of the aortic arch (ao). B: *In vivo* determination of arch-to-blood ratios based on SPECT image quantifications. This ratio was significantly higher in atherosclerotic ApoE$^{-/-}$ than control C57Bl/6J mice for ^{99m}Tc-cAbVCAM1-5 but not for the negative control ^{99m}Tc-cAbBcII10. (* $P<0.05$ vs ^{99m}Tc-cAbBcII10, † $P<0.05$ vs C57BL/6J).

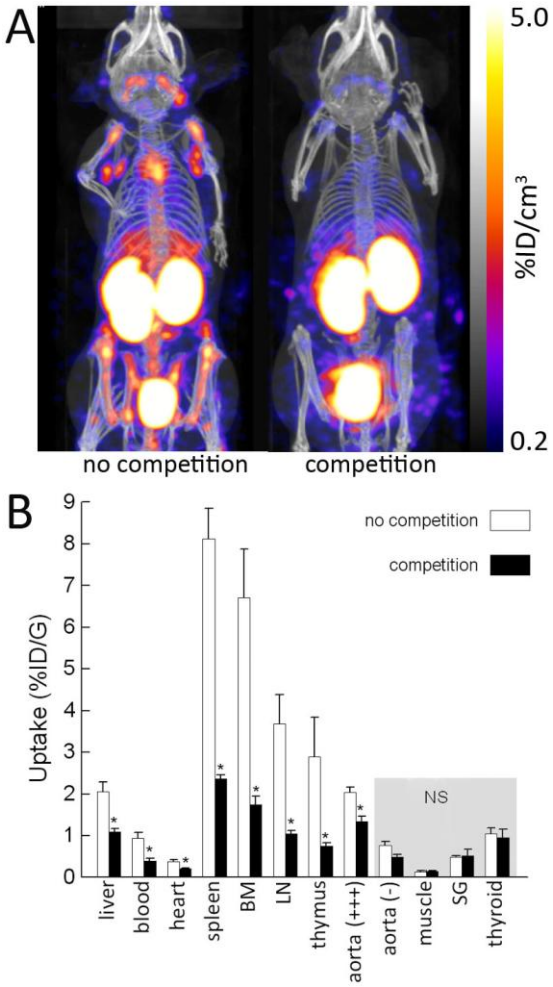

Figure 6. *In vivo* competition study.
^{99m}Tc-cAbVCAM1-5 was injected in ApoE$^{-/-}$ mice either alone (n=4), or together with a 100-fold excess of unlabeled competitor cAbVCAM1-1 (n=6). A: Representative SPECT/CT images. B: *ex vivo* biodistribution at 3h p.i. Competition resulted in significant decreases of ^{99m}Tc-cAbVCAM1-5 uptake in liver, lymphoid tissues and atherosclerotic lesions, thereby demonstrating specificity of the signals. * : P<0.05 vs no competition.